RSC Advances

PAPER

View Article Online
View Journal | View Issue

Cite this: *RSC Adv.*, 2021, **11**, 31272

Polyaniline coated tungsten trioxide as an effective adsorbent for the removal of orange G dye from aqueous media

Abdelghani Hsini, †*[a] Yassine Naciri,†[a] Asmae Bouziani, [b] Nouh Aarab,[a] Abdelilah Essekri,[a] Abdelaziz Imgharn,[a] Mohamed Laabd, [a] J. A. Navío,[c] F. Puga,[c] Rajae Lakhmiri[d] and Abdallah Albourine*[a]

In this work, the core–shell PANI@WO_3 composite was obtained from the reaction of aniline monomer polymerization with WO_3 particles; sodium persulfate was used as an oxidant. Various analytical techniques such as scanning electron microscopy (SEM-EDS), X-ray diffraction (XRD), Fourier transform infrared spectroscopy (FTIR), Brunauer–Emmett–Teller (BET), and X-ray photoelectron spectroscopy (XPS) were used to characterize the as-prepared PANI@WO_3 adsorbent, which well confirmed that the WO_3 particles were coated by polyaniline polymer. The PANI@WO_3 composite was tested as an adsorbent to remove reactive orange G (OG) for the first time. pH, adsorbent dose, contact time, initial dye concentration, and temperature were systematically investigated in order to study their effect on the adsorption process. The experimental findings showed that the PANI@WO_3 composite has considerable potential to remove an aqueous OG dye. Langmuir and Freundlich's models were used to analyze the equilibrium isotherms of OG dye adsorption on the PANI@WO_3 composite. As a result, the best correlation of the experimental data was provided by the Langmuir model, and the maximum capacity of adsorption was 226.50 mg g^{-1}. From a thermodynamic point of view, the OG dye adsorption process occurred spontaneously and endothermically. Importantly, PANI@WO_3 still exhibited an excellent adsorption capability after four regeneration cycles, indicating the potential reusability of the PANI@WO_3 composite. These results indicate that the as prepared PANI@WO_3 composite could be employed as an efficient adsorbent and was much better than the parent material adsorption of OG dye.

Received 27th May 2021
Accepted 13th September 2021

DOI: 10.1039/d1ra04135e

rsc.li/rsc-advances

1. Introduction

Water is a vital component for the existence of all living organisms. Today, most water sources are at risk of being contaminated by various organic and inorganic chemical pollutants from industrial effluents.[1–4] The textile industry discharges effluents containing synthetic dyes and is considered to be the most polluting of all industries. Even at low concentrations, dyes are visible and deemed to be toxic.[5–7] Due to reduced light penetration, accompanied by a reduced amount of dissolved oxygen, dyes have distributed the photosynthetic activity of aquatic life.[8] Hence, the removal of synthetic organic dyes from waste effluents becomes a fundamental environmental challenge. For this purpose, several purification methods including biological, ozonation, membrane filtration, physiochemical, and advanced oxidation treatment processes, are commonly applied to treat dye-laden effluents.[9–14] However, the significant restrictions of these technologies are long operation time, low effectiveness, high sludge production, high cost, *etc.*[15] Adsorption is an alternative wastewater treatment process because of its high performance and ease of operation, as well as the possibility of regeneration.[16–18]

Several adsorbents such as zeolite, cellulose, activated carbon, clay, and so on have been applied to remove dyes from wastewater.[16,18] The reported adsorbents present many drawbacks such as high cost of preparation, regeneration difficulty, and a long time to achieve adsorption equilibrium, thus restricting their large-scale application to treat textile effluents.[8] Therefore, investigations of new recyclable adsorbents are needed.

In recent years, polyaniline (PANI) has attracted much attention. Due to the high electrochemical activity, easiness of protonation reversibility, excellent recyclability of redox,

[a]*Laboratory of Materials and Environment, Faculty of Sciences, Ibn Zohr University, Agadir, Morocco. E-mail: abdelghani.hsini@edu.uiz.ac.ma; albourine.abdallah@gmail.com*

[b]*Chemical Engineering Department, Middle East Technical University, Ankara, Turkey*

[c]*Instituto de Ciencia de Materiales de Sevilla, Centro Mixto Universidad de Sevilla-CSIC, Américo Vespucio 49, 41092 Sevilla, Spain*

[d]*Laboratory of Chemical Engineering and Valorization Resources, Faculty of Sciences and Techniques, Abdelmalek Essaadi University, Tangier, Morocco*

† These authors contributed equally to this work.

environmental stability, easy preparation, and low cost.[19,20] Moreover, owing to the presence of large amounts of amine and imine functional groups in the polymer chains, PANI and its composites can be used as adsorbents to remove anionic and cationic dyes.[21–23] However, the major drawback of PANI usage as an adsorbent is the low mass density making it hard to settle and limiting its usefulness as an absorbent.[23,24]

Recently, metal oxides have been reported to hold immense potential for adsorptive remediation of wastewater. This can be attributed to their large surface area, thermal stability, porous structures, low toxicity, easy recovery, and the presence of Lewis acid–base sites, O-vacancy sites, and defects on the surface.[25,26] Among these metal oxides, tungsten trioxide (WO_3) nanoparticles have attracted considerable studies properties such as small energy band gap (from 2.4 to 2.8 eV), stable physicochemical properties, non-toxicity, and resistance to photocorrosion. However, their adsorption properties are significantly less investigated.[27,28]

In general, the addition of inorganic materials to conductive polymers alters the physical and chemical properties of the components, and resulting composites display synergic or complementary behaviors.[29–31] For example, the results of the study conducted by S. M. Ali *et al.* showed that SiO_2, TiO_2, Al_2O_3, and Fe_3O_4 oxides nanoparticles covered by PANI are efficient in adsorbing reactive congo red dye.[32] Similarly, S. Agarwal *et al.* reported using polyaniline-zirconium oxide nanocomposite as an efficient adsorbent to remove MB dye from an aqueous solution.[29] Hence, a composite of tungsten trioxide (WO_3) with PANI is expected to display tremendous results for the effective abatement of dyes from water.

No former study has been conducted to remove OG dye by PANI@WO_3 composite to our best knowledge. Thus, the present study would serve as an essential contribution to filling this knowledge gap. Herein, the goals of this study are to (1) synthesize PANI@WO_3 composite and use it as scavenger-type material for the removal of OG dye from aqueous solution; (2) investigate the effect of various operating parameters such as adsorbent dose, pH, initial dye concentration, contact time, and temperature in batch experiments on OG removal; (3) characterize the chemical, morphological and physical properties of the PANI@WO_3 composite before and after adsorption of OG dye *via* FTIR, XRD, XPS, SEM, EDS, TEM, and BET techniques; (4) delineate the kinetics and thermodynamics of OG dye adsorption; and (5) discuss the adsorption mechanism of chromium(VI) onto PANI@WO_3 composite using XPS analysis.

2. Experimental

2.1 Materials and chemicals

Sigma-Aldrich supplied all the chemical reagents used in this paper, ammonium tungstate ($(NH_4)_6H_5[H_2(WO_4)_6]\cdot H_2O$, 99%), aniline ($C_6H_5NH_2$, 99%), sodium persulfate ($Na_2S_2O_8$, 99%), orange G (OG), hydrochloric acid (HCl, 36%), sodium hydroxide (NaOH), acetone (C_3H_6O) and ethanol (CH_3CH_2OH) were of analytical grade, and no extra purification was needed. Distilled water was used for the preparation of stock solutions as well as for the materials synthesis and adsorption experiments.

2.2 Fabrication of PANI@WO_3 nanocomposite

The WO_3 powder used in this study was synthesized according to the procedure described by Li *et al.*[33] The *in situ* polymerization of aniline monomer was applied to synthesize PANI@WO_3 nanocomposite with core–shell structure in the presence of a host matrix (WO_3 particles). First, 1 g of WO_3 powder was dissolved in 100 mL of HCl (1 M) *via* sonication for 30 min. Next, a recently distilled aniline (1 mL) was dropped into the mixture and then sonicated for 1 h. Then, under stirring, 50 mL of HCl (1 M) containing the oxidant sodium persulfate (with a monomer/oxidant molar ratio of 1 : 2) was added drop by drop and kept under stirring for 12 h at ambient temperature. The resulting mixture was filtered, and the collected product was washed numerous times with water, ethanol, and acetone in order to eliminate the excess of oligoaniline and oxidant. Finally, the prepared PANI@WO_3 nanocomposite material was kept overnight at 80 °C.

2.3 Characterization of the adsorbent

The physicochemical properties of the PANI@WO_3 composite were measured and evaluated by numerous characterization methods. The crystal structure of WO_3 and PANI@WO_3 composite was characterized by X-ray powder diffraction (XRD) analysis *via* an EMPYREAN PANALYTICAL diffractometer equipped with a copper X-ray (wavelength of 1.54×10^{-10} m, voltage of 45 kV, and current intensity of 35 mA). The XRD data were recorded over a 2θ angle range of 10–80°. The microstructure of the as-prepared adsorbent samples was recorded on a transmission electron microscope (Philips CM 200 microscope). FTIR spectroscopy (ALPHA-Bruker Optics, Germany) with KBr pellets scanning in the 400 to 4000 cm^{-1} frequency array was used to identify the characteristic chemical bond of the WO_3 particles prior to and after PANI coating. The analysis of the chemical composition of the PANI@WO_3 surface before and after OG dye adsorption was made by X-ray photoelectron spectroscopy (XPS) (SPECS spectrometer). The obtained spectra were standardized to C 1s peak at 284.6 eV. The morphology and microstructure of WO_3 and PANI@WO_3 before and after OG adsorption were documented on a scanning electron microscope (SEM, JEOL, JSMIT200) attached with a dispersive energy X-ray (EDS) analysis. A Micromeritics ASAP 2420 accelerated surface area and porosimetry system, with a liquid-nitrogen cooling bath (−195.78 °C), was used to measure the BET specific surface area.

The point of zero charges (pH_{PZC}) corresponds to the pH value of the solution surrounding the adsorbent in which the positively charged active sites were equal to the negative ones on the adsorbent surface. The pH_{PZC} of PANI@WO_3 was calculated *via* the potentiometric titration procedure described in our previous article.[34]

2.4 Batch experiments

The adsorption experiments were performed in a batch reactor. The adsorption behavior of PANI@WO_3 composite toward OG dye was experimentally investigated under different operational settings, including the amount of adsorbent (0.125–1 g L^{-1}),

solution pH (2–10), adsorption time (0–240 min), initial concentration of dye (0.025–0.400 g L^{-1}) and temperature (298–328 K). The influence of these parameters on the efficiency of adsorption was investigated, changing one parameter at a time. After each adsorption experiment, the PANI@WO_3 was removed from the solution *via* a Millipore filter (0.45 μm). The OG concentration prior and after adsorption was obtained *via* a UV2300 spectrophotometer and following the band of adsorption at 476 nm. The percentage absorbed R (%), and the capacity of adsorption Q_e (mg g^{-1}) was obtained from the below formulas:[34]

$$R\ (\%) = \frac{(C_0 - C_e)}{C_0} \times 100 \quad (1)$$

$$Q_e = \frac{(C_0 - C_e)}{m} \times V \quad (2)$$

C_0 (mg L^{-1}) is the OG initial concentration; C_e (mg L^{-1}): OG concentration at equilibrium; m (g) is the quantity of the PANI@WO_3 composite, and V (L) is the volume of OG.

2.5 PANI@WO_3 regeneration

The regeneration experiment was performed for 6 h using a 0.5 M NaOH eluent solution used for the desorption of OG dye from PANI@WO_3. A successful regeneration was obtained after washing PANI@WO_3 composite with distilled water and redoping with 1 M HCl for an additional adsorption cycle. In this study, four adsorption/desorption cycles were conducted.

3. Results and discussion

3.1 Characterization of the adsorbent

XRD is a central technique for the determination of the structure and composition of obtained composites. Fig. 1 displays the XRD patterns of WO_3 and PANI@WO_3 composite. The characteristic diffraction peaks appeared at the peaks at 2θ = 23.09, 23.51, 24.30, 26.66, 28.85, 33.35, and 34.09 refer to (002), (020), (200), (120), (112), (022) and (202) diffraction planes of WO_3 consistent with the monoclinic structure and are in accordance with JCPDS file 01-072-0677. The lattice constants a = 7.3060 Å, b = 7.5400 Å and c = 7.6920 Å for WO_3. The addition of PANI did not alter the peaks' position or shapes; thus, the XRD patterns of the PANI@WO_3 composite are similar to WO_3. Therefore, the PANI did not change the crystal structure of WO_3, and no peaks belonging to PANI were observed because of its amorphous nature in the composite. Analogous results were described for other PANI-based composites.[35–37]

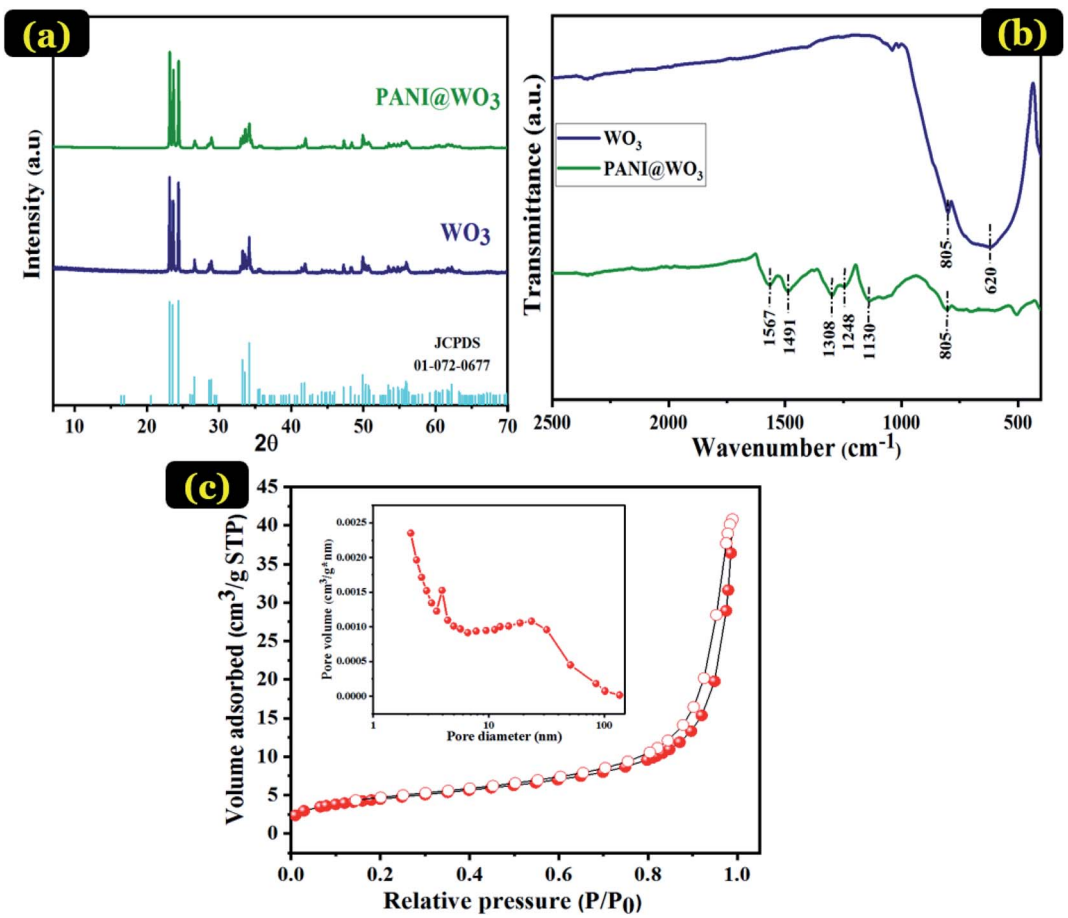

Fig. 1 XRD patterns of WO_3 and PANI@WO_3 composite (a), FTIR spectra of WO3 and PANI@WO3 composite (b), N_2 adsorption–desorption isotherms and the conforming pore size distribution plot of PANI@WO_3 composite (c).

The FT-IR spectroscopy further identifies the structural information and chemical component of the PANI@WO_3 composite. For comparison, the spectra of WO_3 was also recorded and shown in Fig. 1(b). The characteristic peaks of WO_3 situated at 620 and 805 cm^{-1} are recognized as the stretching vibrations of O–W–O.[38] The adsorption peak at 805 cm^{-1} was also observed in the spectrum of PANI@WO_3, which demonstrated the presence of WO_3 in the PANI@WO_3 composite. Moreover, the FT-IR spectrum of the PANI@WO_3 composite comprises new bands in the range 500–1600 cm^{-1}, characteristic of PANI stretching. The typical peak at 1130 cm^{-1} is related to the anion used as a dopant (Cl-PANI). The vibration peaks of C=C and C–N stretching modes in Ar–NH–Ar are situated at 1248 and 1308 cm^{-1}, respectively. Furthermore, the bands in the frequency range of 1491–1567 cm^{-1} are characteristic of C=C in the structure of benzenoid and quinoid stretching vibrations.[39] The band at approximately 805 cm^{-1} matches the C–H bending vibration out of the plane of the *para* disubstituted benzene rings.[31,40] These bands confirm the structure of polyaniline in its emeraldine salt form. The FT-IR

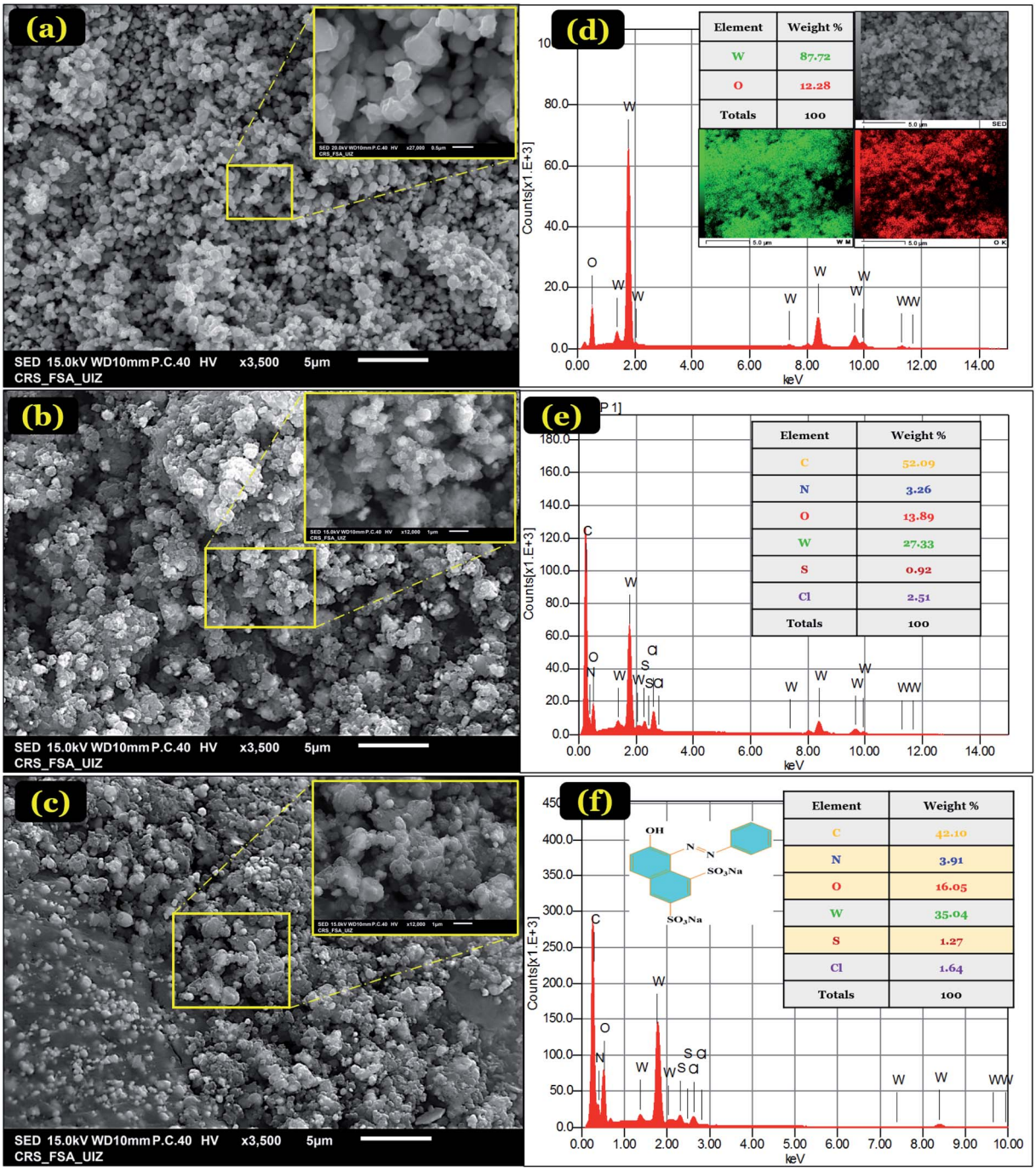

Fig. 2 SEM images of WO_3 (a), PANI@WO_3 (b), PANI@WO_3-OG (c). EDS elemental analysis of WO_3 (d), PANI@WO_3 (e), and PANI@WO_3-OG (f).

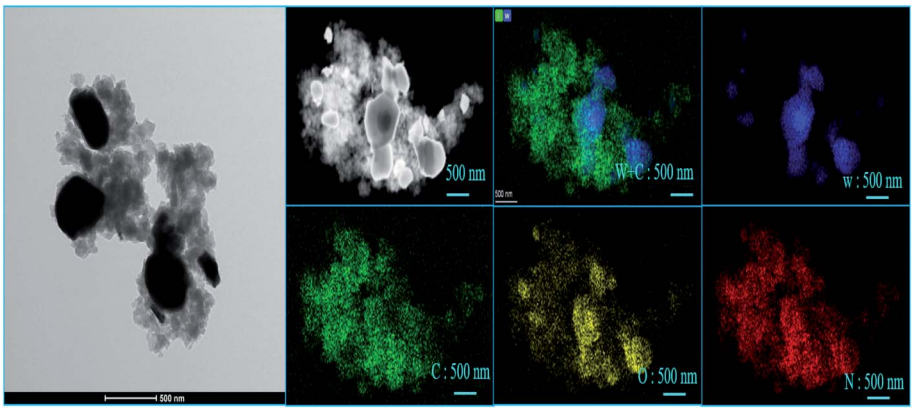

Fig. 3 TEM image, and tungsten (W), carbon (C), oxygen (O), nitrogen (N), represented by different colors, blue, green, yellow, and red, respectively, of elements mapping image of PANI@WO_3.

findings provide substantial proof of the successful formation of the PANI@WO_3 composite.

The BET surface is an essential property of the adsorbent, which influences the adsorption performance. Pore diameter distribution also has a significant impact on the adsorption process performance. BET method can determine the specific surface area of particles, the average pore radius, and the total pore volume of the adsorbent. Fig. 1(c) exhibits the nitrogen adsorption–desorption isotherms of PANI@WO_3 composite with an inset showing its conforming Barrett–Joyner–Halenda (BJH) pore size distribution. From Fig. 1(c) and according to the IUPAC classification, PANI@WO_3 composite displays a type IV isotherm consisting of a mesoporous material.[41] The pore diameter is between 2 and 4 nm (Fig. 1(c)), which confirms the mesoporous structure of the PANI@WO_3 composite. The prepared PANI@WO_3 composite has shown specific surface area and total pore volume of 16.28 $m^2\ g^{-1}$ and 0.04 $cm^3\ g^{-1}$ using the BET method. This surface area is higher or comparable to many polymer based composite adsorbents like polyaniline/SiO_2 nanocomposite (13.36 $m^2\ g^{-1}$)[42], https://www.sciencedirect.com/science/article/pii/S1350417718312501 – b0080, polyaniline/TiO_2 (11.60 $m^2.\ g^{-1}$).[43]

Fig. 2(a–c) displays the morphology of the synthesized WO_3, PANI@WO_3, and PANI@WO_3 after OG adsorption. WO_3 nanoparticles show a uniform structure having approximately 500 nm diameter as well as a few agglomerations. While PANI@WO_3 exhibits pores that resulted from PANI coating on the surface of WO_3 and confirms the core–shell morphology of the PANI@WO_3 composite. The infiltration and diffusion of adsorbate to the internal PANI@WO_3 surface are eased by pores formation. Fig. 2(c) shows a notable modification in the surface of the PANI@WO_3 composite after the adsorption of OG. The surface of the PANI@WO_3 composite reached the saturation point.

EDS analysis of WO_3, PANI@WO_3, and PANI@WO_3 was performed after the OG adsorption, and the outcomes are displayed in Fig. 2(d–f). The elemental compositions are specified in the corresponding tables. The WO_3 EDS spectrum (Fig. 2(d)) shows mostly tungsten and oxygen. Fig. 2(e) shows the presence of W and O atoms belonging to WO_3 and the chloride (Cl), sulfur (S), and nitrogen (N) elements corresponding to PANI.

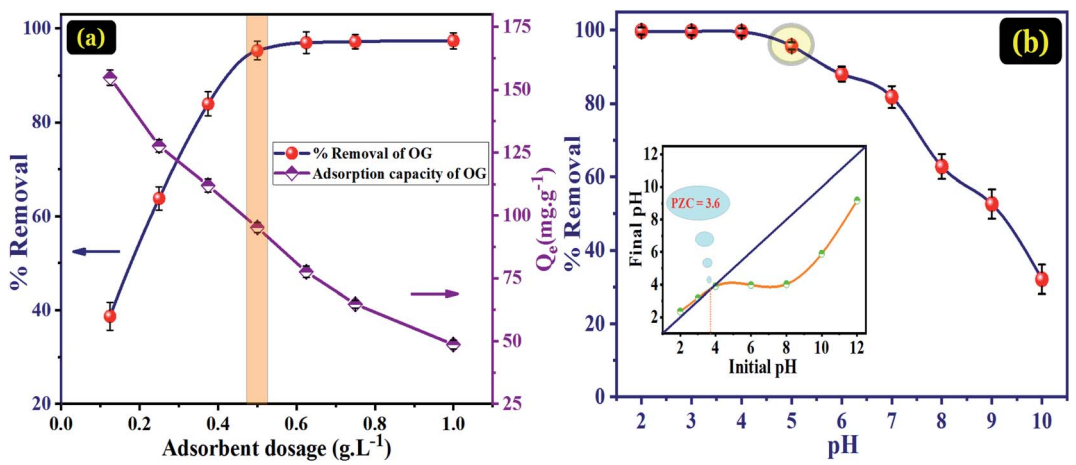

Fig. 4 (a) Effect of adsorbent dose on adsorption capacity and percentage removal of OG dye ($C_0 = 0.050$ g L^{-1}, pH = 5, $t = 120$ min and $T = 298$ K). (b) pH solution effect on the removal of OG *via* PANI@WO_3 ($C_0 = 0.050$ g L^{-1}, $t = 120$ min, adsorbent dose = 0.5 g L^{-1} and $T = 298$ K).

Additionally, no impurity peaks were detected, confirming the purity of the synthesized PANI@WO_3 composite. An increase in O, S, and N was noticed upon the OG adsorption (Fig. 2(f)). In contrast, a decrease in the content of C was observed in PANI@WO_3. These outcomes were anticipated as a consequence of the OG adsorption on the PANI@WO_3 surface.

The typical TEM images of PANI@WO_3 core–shell composite are given in Fig. 3. The morphological observations of the PANI@WO_3 composite revealed that the composite consists of well WO_3 particles with an average diameter of 500 nm, which are dispersed and attached to the PANI chain. It was observed that the dark core is the WO_3 particles, and the light colored shell is the PANI in the nanocomposite. The outcome of the TEM analysis confirms the successful synthesis of the PANI@WO_3 composite.

The elemental mappings for PANI@WO_3 composite were also performed. The elemental mapping confirmed the chemical composition of PANI@WO_3 composite with the presence of tungsten (W), carbon (C), oxygen (O), nitrogen (N), represented by different colors, blue, green, yellow, and red, respectively, as shown in Fig. 3. The investigation, as mentioned above, can support the successful coating of PANI on WO_3.

3.2 Adsorption analysis

3.2.1 Adsorbent dose and pH effects. The influence of adsorbent dosage on adsorption capacity and percentage removal of OG dye is shown in Fig. 4(a). It has been found that an increase in the dosage of adsorbent from 0.1 to 0.5 g L^{-1} leads to a noteworthy increase in the percentage of removal of OG dye (from 38 to 95%). This adsorption inclination may be due to the increased number of available binding sites.[16] Above an adsorbent of 0.5 g L^{-1}, the removal efficiency remained constant. However, when the PANI@WO_3 dose increased, the capacity of adsorption decreased from 154.85 to 48.68 mg g^{-1}, indicating that the PANI@WO_3 quantity had to be checked through the OG removal process.[44]

To some extent, the removal efficiency of OG dye could be enhanced as the number of active sites augmented, and the dose optimum of adsorbent was 0.5 g L^{-1}. After this optimal adsorbent dose, it was found that the efficiency of removal did not improve as more adsorbent was added. Therefore, it can be concluded that 0.5 g L^{-1} of PANI@WO_3 is the optimum adsorbent dose used to perform the following batch experiments.

The pH of a solution is an essential parameter to understand the adsorption phenomenon by modifying the adsorbent surface charge and the protonation state of the adsorbate molecules. Therefore, the pH influence on the adsorption of OG and PZC of PANI@WO_3 was investigated in a pH array of 2–10. From Fig. 4(b), the percentage of OG dye removal remained very high (>95%) in the pH range of 2–5 and then decreased progressively as the initial solution pH increased. The pK_a of OG are 1.0 and 11.5 for the deprotonation/ionization of the two sulfonic (–SO_3H) groups and naphthalene hydroxy (–OH) function, respectively.[34] Therefore, the OG molecules are charged negatively over the entire established pH array. The pH_{PZC} of PANI@WO_3 is 3.6 (Fig. 4(b)). Thus, the PANI@WO_3 surface charge is positive at pH < pH_{PZC} and negative once pH > pH_{PZC}. The OG adsorption can be due to the electrostatic interactions between OG molecules and the PANI@WO_3 composite surface. At pH < 4, the high adsorption performance was attributed to the electrostatic attractions between the anionic OG molecules and the positive charge of the PANI@WO_3 surface. Yet, at pH > 4, the adsorption decreased due to a decrease in the number of sites charged positively, inhibiting the OG adsorption on the PANI@WO_3 surface.[45] The OG adsorption efficiency observed at pH > 4 could be explained by π–π interactions between OG dye molecule and PANI. Therefore, the optimal pH value of 5 was selected and used in subsequent OG dye adsorption experiments.

3.2.2 Kinetics study. The influence of adsorption time on the OG removal by PANI@WO_3 was investigated, and the results are given in Fig. 5(a). The OG capacity of adsorption onto PANI@WO_3 composite increased rapidly in the first 30 min, then slowly, and the equilibrium was reached within 120 min. At the early stages of the adsorption process, the faster adsorption rate could be presumably attributed to a significant gradient of OG concentration at the solution/PANI@WO_3 interface. As the adsorption time extended, the active sites

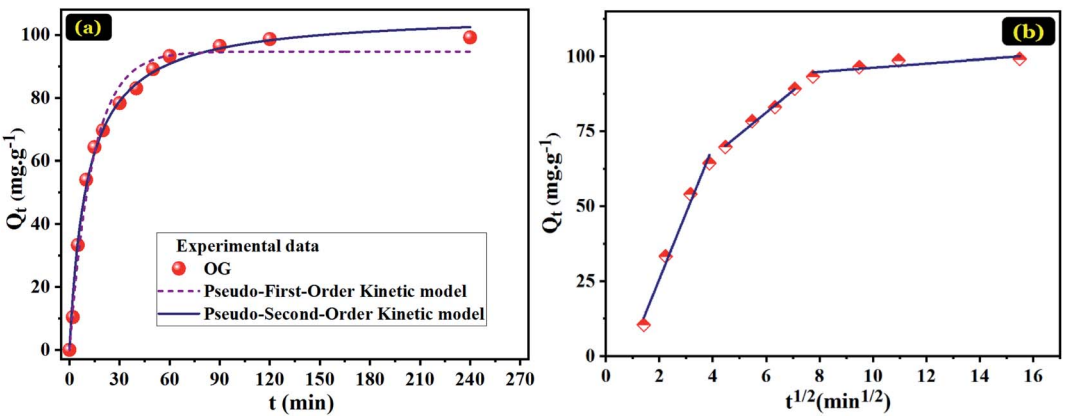

Fig. 5 Plots for OG adsorption on PANI@WO_3 (C_0 = 0.050 g L^{-1}, pH = 5, adsorbent dose = 0.5 g L^{-1} and T = 298 K). Pseudo-first and pseudo-second order (a) and Weber–Morris intra-particle diffusion (b).

Table 1 The adsorption of OG onto PANI@WO_3 kinetic parameters

		Pseudo-first order			Pseudo-second order		
	$Q_{e.exp}$ (mg g^{-1})	k_1 (min^{-1})	$Q_{e.1}$ (mg g^{-1})	R^2	k_2 (g mg^{-1} min^{-1})	$Q_{e.2}$ (mg g^{-1})	R^2
PANI@WO_3	99.16	0.07203	94.64	0.9864	8.7698×10^{-4}	106.98	0.9947

	Weber–Morris model								
	Initial linear portion			Second linear portion			Third linear portion		
	$k_{int.1}$	C_1	R^2	$k_{int.2}$	C_2	R^2	$k_{int.3}$	C_3	R^2
PANI@WO_3	22.079	−18.452	0.9850	7.311	37.405	0.9935	0.686	89.385	0.7155

gradually filled, leading to decreased OG removal rate, and the adsorption efficiency plateaued (equilibrium state).

To understand the adsorption mechanisms of OG on the PANI@WO_3 composite, the adsorption kinetic data were fitted with pseudo-first-order and pseudo-second-order kinetic models (Fig. 5(a)). The equations of these kinetic models are given as follows:[31]

Pseudo-first-order model:

$$Q_t = Q_e(1 - e^{-k_1 t}) \quad (3)$$

Pseudo-second-order model:

$$Q_t = \frac{Q_e^2 k_2 t}{1 + Q_e k_2 t} \quad (4)$$

where k_1 (min^{-1}) is the rate constant of the pseudo-first-order and k_2 (mg g^{-1} min^{-1}) the rate constant of the pseudo-second-order. Q_e (mg g^{-1}) adsorbed amounts at equilibrium and Q_t (mg g^{-1}) adsorbed amounts at time t (min).

The fitting parameters of the kinetic models are recorded in Table 1. On the basis of the correlation coefficient (R^2) values, the pseudo-second-order model (0.9947) is more fitted to the OG adsorption kinetic data than the pseudo-first-order model (0.9864). Besides, the adsorbed amount obtained from the pseudo-second-order model is nearer the experimental one. Therefore, the OG adsorption process on the PANI@WO_3 composite is following the pseudo-second-order kinetic rate.

The mass transfer mechanism of OG molecules between the aqueous phase and PANI@WO_3 surface was tested using an intra-particle diffusion model. The intraparticle diffusion model is defined as follows:[31]

$$Q_t = k_{int} t^{1/2} + C \quad (5)$$

where k_{int} (mg g^{-1} $min^{-1/2}$) represents the intraparticle diffusion rate constant. C (mg g^{-1}) is a constant related to the thickness of the boundary layer. Q_t (mg g^{-1}): the amount adsorbed at time t (min).

Fig. 5(b) shows the Q_t *vs.* $t^{1/2}$ plots for OG adsorption onto PANI@WO_3 composite; the corresponding parameters are summarized in Table 1. The graphical representation clearly indicates that the OG dye transfer from bulk liquid to solid material surface sites is a three-stage process. The first stage corresponds to the mobility of OG from bulk liquid to the

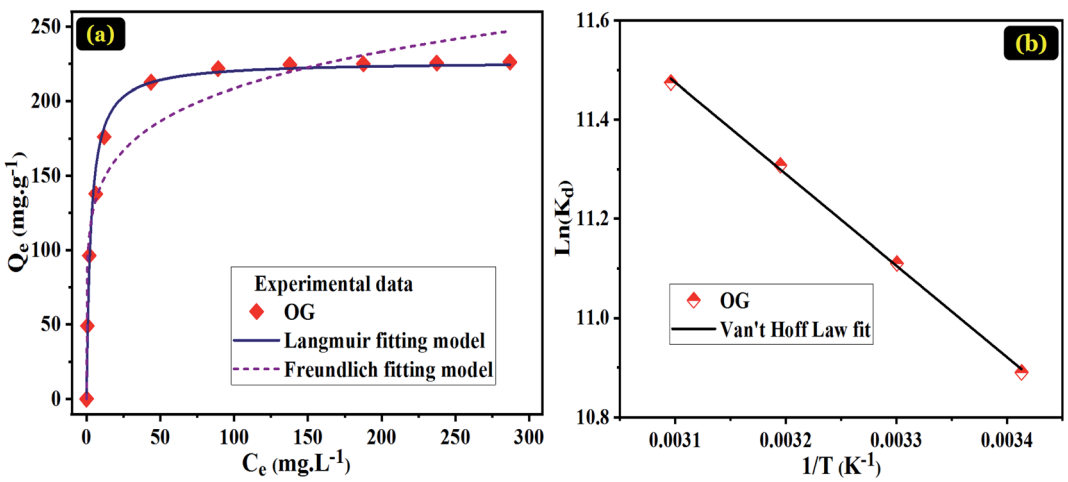

Fig. 6 (a) Non-linear Langmuir and Freundlich isotherm plots for the adsorption of OG on the PANI@WO_3 (pH = 5, t = 240 min, adsorbent dose = 0.5 g L^{-1} and T = 298 K) and (b) Van't Hoff plot for thermodynamic parameters determination.

Table 2 Langmuir and Freundlich isotherm formulas and the conforming parameters for OG adsorption onto PANI@WO_3

		Langmuir $Q_e = \frac{Q_{max} K_L C_e}{1 + K_L C_e}$			Freundlich $Q_e = K_F C_e^{1/n}$		
	Q_{exp} (mg g^{-1})	Q_{max} (mg g^{-1})	K_L (L mg^{-1})	R^2	n_f	K_F (mg g^{-1})	R^2
PANI@WO_3	226.22	*226.50*	*0.3455*	*0.9884*	*6.229*	*99.573*	*0.9345*

Table 3 The uptake capacity of PANI@WO_3 for OG comparison with other adsorbents described in the literature

	Maximum adsorption capacity (mg g^{-1})	
Adsorbent	OG	Reference
ZnO-AC	153.8	47
Cts(*x*)-*g*-PNVP	63.7	48
AC from coffee grounds	100	49
PANI@AS biocomposite	190.98	34
Monoamine-modified silica	36.3	50
FSMD MNPs	109.1	51
PANI@OFI-A	303.94	52
PANI@WO_3 composite	226.50	Current study

external surface of PANI@WO_3 composite. This stage is characterized by a significant OG dye mass transfer owing to the higher mass flow rate. The second stage represents the diffusion of OG dye molecules inside the mesopores of the PANI@WO_3 composite. The diffusion rate of this step is inferior to that of the first one and is coordinated mainly by pore diffusion.[31] The third stage is credited to ultimate adsorption equilibrium due to the eventual saturation of adsorbent surface sites.[46]

3.2.3 Adsorption isotherm and thermodynamic parameters. Isotherm of adsorption study is a crucial feature to anticipate OG distribution at the interface between the liquid phase and adsorbent surface.[31] To understand the adsorption mechanism between OG dye and PANI@WO_3 surface, the experimental data of adsorption was regressively simulated with Langmuir and Freundlich isotherms models; outcomes are given in Fig. 6(a) and Table 2. On the basis of the obtained coefficient of regression (R^2), it is clear that the Langmuir model is better suited to explain the adsorption of OG on PANI@WO_3 than the Freundlich model. Due to the uniform shape, the adsorption of OG is dominated by monolayer adsorption on the surface of PANI@WO_3.[31] The adsorption capacity optimal for PANI@WO_3 adsorbent calculated from the Langmuir model was 226.50 mg g^{-1}, which is near the adsorption value obtained experimentally (226.22 mg g^{-1}). The OG maximum capacity of adsorption on PANI@WO_3 was compared with already reported adsorbents, as summarized in Table 3. Obviously, the PANI@WO_3 displayed a remarkable OG adsorption capacity rather than earlier described adsorbents. Hence, the PANI@WO_3 composite is an excellent adsorbent to remove OG from an aqueous solution.

Indicative symbols: Q_{max} (mg g^{-1}) the maximum adsorption capacity and C_e (mg L^{-1}) concentration of OG at equilibrium; K_L (L mg^{-1}), K_F (mg g^{-1}), and n_F represent the constant of Langmuir isotherm associated with the adsorption heat, constant of Freundlich isotherm relating the adsorption density and the intensity of adsorption, respectively.

The thermodynamic study was achieved to investigate the nature of the OG dye adsorption process onto PANI@WO_3 composite (Fig. 6(b)). The thermodynamic parameters including enthalpy change (ΔH°), Gibb's free energy change (ΔG°), and entropy change (ΔS°) were calculated by eqn (6) and (7):[53]

$$\Delta G^\circ = -RT \ln K_d \quad (6)$$

$$\ln K_d = \frac{\Delta S^\circ}{R} - \frac{\Delta H^\circ}{RT} \quad (7)$$

T and R denote the absolute temperature (°K) and the constant of an ideal gas (8.314 J K^{-1} mol^{-1}). K_d signifies the constant of adsorption at equilibrium stated as: $K_d = \frac{Q_e}{C_e} \times \rho$. ρ (1000 mg L^{-1}) denotes the density of water.

The thermodynamic parameters results are summarized in Table 4. The negative values of ΔG° suggest that the nature of the adsorption of OG over the PANI@WO_3 surface is a spontaneous process. Besides, the absolute values of ΔG° augmented with the increase of temperature, suggesting an enhanced spontaneity at higher temperatures. The magnitude of ΔG° (less than 40 kJ mol^{-1}) evidenced that the OG dye adsorption is a physisorption type.[34] The positive ΔH° confirmed that the adsorption of OG onto PANI@WO_3 is an endothermic process. Moreover, the positive ΔS° value reveals a rise in the unpredictability at the solution/PANI@WO_3 interface through the sorption process, reflecting the excellent affinity of PANI@WO_3 composite towards OG dye molecules.

Table 4 The quantities of ΔG°, ΔH°, and ΔS° for adsorption of OG on the PANI@WO_3

	ΔH° (kJ mol^{-1})	ΔS° (J mol^{-1} K^{-1})	ΔG° (kJ mol^{-1})			
			298 K	308 K	318 K	328 K
PANI@WO_3	15.86	143.77	−26.96	−28.43	−29.88	−31.27

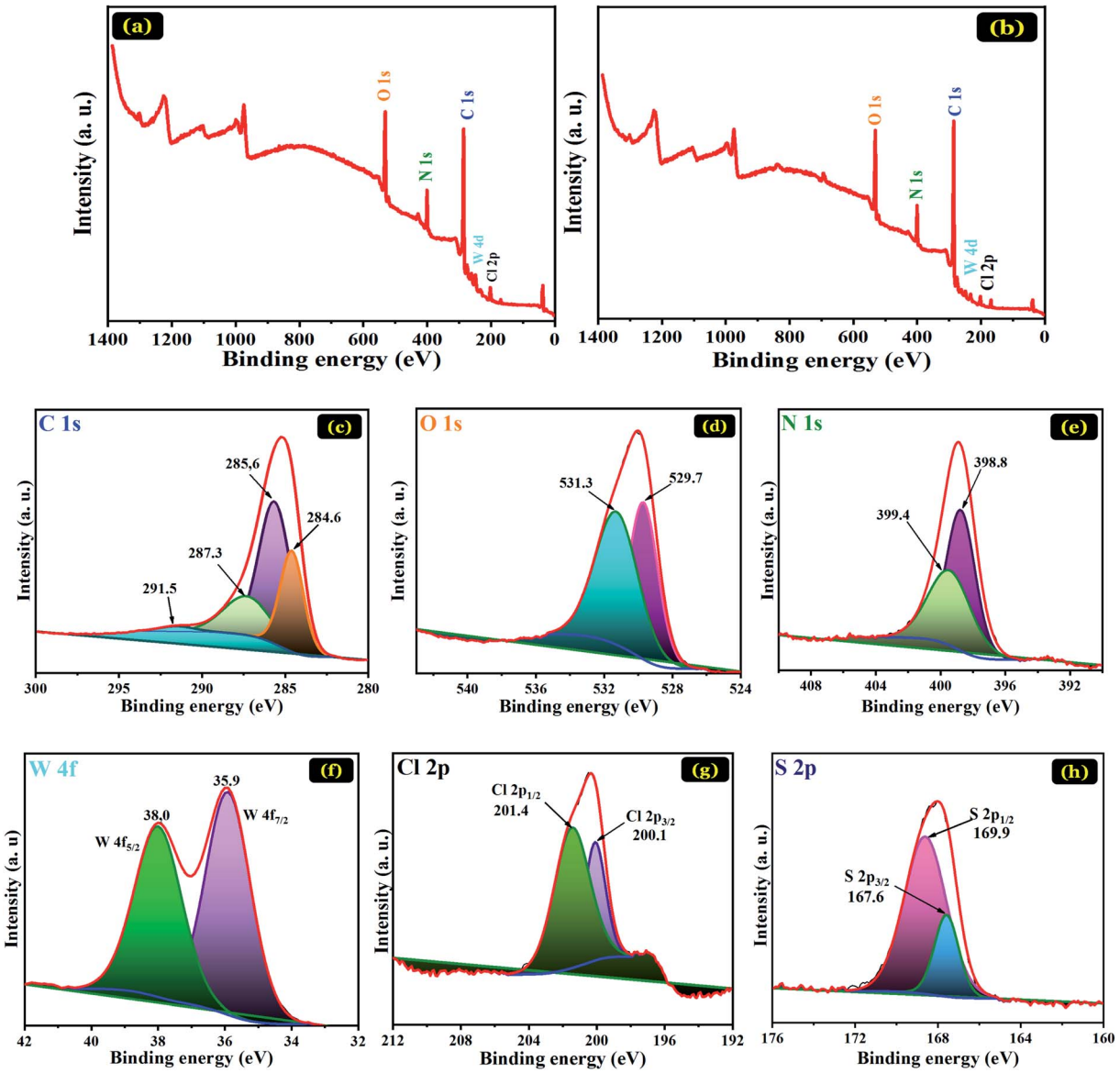

Fig. 7 XPS survey spectrum (a), high-resolution XPS spectra of C 1s (c), O 1s (d), N 1s (e), W 4f (f), Cl 2p (g) of PANI@WO_3 prior adsorption of OG. XPS survey spectrum (b), and high-resolution XPS spectra of S 2p (h) of PANI@WO_3 after OG dye adsorption.

3.2.4 XPS analysis and mechanism of adsorption. XPS technique was used to characterize the PANI@WO_3 prior and after OG adsorption. The spectral figures for C 1s, O 1s, N 1s, W 4d, Cl 2p, and S 2p of PANI@WO_3 are shown in Fig. 7. The conforming elemental examination is given in Table 5. The presence of PANI and WO_3 nanoparticles were confirmed by the presence of N 1s and W 4d peaks. Fig. 7(c) displays the C 1s spectrum where the peaks at 284.6, 285.6, 287.3, and 291.5 eV are characteristically related to the presence of C–C or C–H, C–N, C=N, and π–π (satellite) links in the PANI.[31] The core-level spectrum of the N 1s (Fig. 7(e)) displays two peaks: 398.8 and 399.4 eV consistent respectively with the amine (–NH–) and doped amine (–NH^+/–N^+=) groups of the polyaniline.[31] Therefore, we can conclude that the doped PANI polymer (emeraldine salt form) was effectively placed on the surface of WO_3 particles. After OG dye adsorption, the XPS spectra signal of sulfur element was detected at a binding energy of 168 eV (Fig. 7(h)), indicating the adsorption of OG dye on the PANI@WO_3

Table 5 Chemical composition of PANI@WO_3 prior and after adsorption of OG

	Atomic concentration (%)	
Element	PANI@WO_3	PANI@WO_3-OG
C	70.70	72.30
O	16.21	14.39
N	9.523	9.279
W	0.57	0.25
Cl	2.30	1.69
S	Atomic% lower than the detection limit	1.98

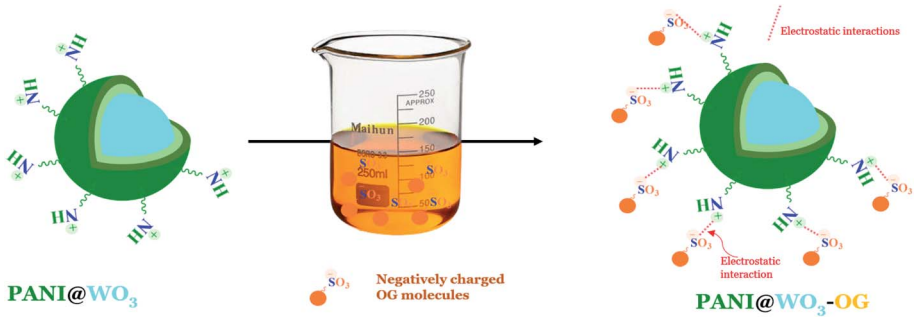

Fig. 8 Illustration of the adsorption mechanism of OG dye onto PANI@WO_3 composite.

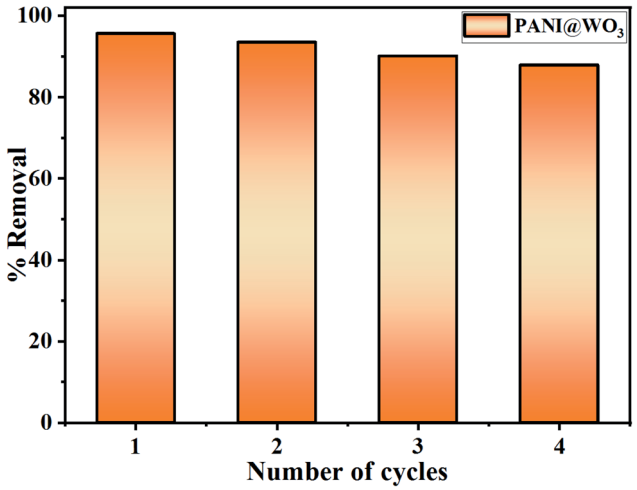

Fig. 9 Recyclability test of PANI@WO_3 for OG dye removal.

composite. Besides, there was no significant change in the peaks associated with the elements of PANI@WO_3 composite after interaction with OG dye. This means that the OG dye was adsorbed on the PANI@WO_3 through physical interactions, which is consistent with the thermodynamic study. Moreover, the investigation of the effect of pH on the adsorption process (Section 3.2.1. Effects of adsorbent dose and pH) further confirmed that both electrostatic interactions and π–π interactions are involved in the OG dye adsorption mechanism.[34,51] In light of the above discussion, a proposed OG dye adsorption mechanism on the PANI@WO_3 composite is schematized in Fig. 8.

3.2.5 Regeneration of PANI@WO_3 composite. The regeneration of PANI@WO_3 using NaOH eluent for recovery of OG dye was investigated up to four times. The results of the repeated use experiments are exhibited in Fig. 9. It was noticed that the uptake ability of PANI@WO_3 composite to remove OG dye from aqueous solutions was still kept at about 87.90% after four cycle uses. Therefore, it was concluded that PANI@WO_3 composite has excellent reusability and subsequently represents an alternative adsorbent for effective clean-up of wastewater containing OG dye.

4. Conclusion

A new PANI@WO_3 composite was successfully fabricated and tested to remove OG from an aqueous solution using the adsorption properties of the composite. The PANI@WO_3 composite formation was confirmed by XRD, FT-IR, SEM-EDS, XPS, BET, and TEM analysis. The results confirm the quickness and efficiency of the adsorbent to adsorbs OG dye (>95%). The binding mechanism of OG dye on the PANI@WO_3 surface was proposed to be the collaboration of electrostatic interactions and π–π interactions. The maximum adsorption capacity of PANI@WO_3 for OG dye reached 226.5 mg g^{-1}, which is greater than those of other adsorbents described in the literature. A table of comparative results between our results and those of other authors would be welcome. The adsorption process follows the pseudo-second-order kinetic model, and the Langmuir model is suitable to define adsorption equilibrium. The thermodynamic parameters revealed that the OG adsorption onto PANI@WO_3 is spontaneous and endothermic. The regeneration study demonstrated that the PANI@WO_3 composite has potential reusability for efficient OG removal up to four consecutive cycles. Overall, the experimental findings reported in this study demonstrated that the as-prepared PANI@WO_3 composite is promising adsorbent material for efficient clean-up of OG dye from textile effluents.

Conflicts of interest

There are no conflicts to declare.

References

1 M. Benafqir, A. Hsini, M. Laabd, T. Laktif, A. Ait Addi, A. Albourine and N. El Alem, *Sep. Purif. Technol.*, 2020, **236**, 116286.
2 Y. Abdellaoui, H. Abou Oualid, A. Hsini, B. El Ibrahimi, M. Laabd, M. El Ouardi, G. Giácoman-Vallejos and P. Gamero-Melo, *Chem. Eng. J.*, 2021, **404**, 126600.
3 A. Hsini, Y. Naciri, M. Laabd, M. El Ouardi, Z. Ajmal, R. Lakhmiri, R. Boukherroub and A. Albourine, *J. Mol. Liq.*, 2020, **316**, 113832.
4 Y. Naciri, A. Bouddouch, B. Bakiz, A. Taoufyq, M. Ezahri and A. Benlhachemi, *Mater. Today: Proc.*, 2020, **22**, 48–51.

5 S. Ferraa, Y. Naciri, A. Hsini, H. Barebita, A. Bouziani, A. Albourine, A. Nimour and T. Guedira, *Chem. Phys. Lett.*, 2021, **763**, 138173.
6 Y. Naciri, A. Hsini, Z. Ajmal, A. Bouddouch, B. Bakiz, J. A. Navío, A. Albourine, J.-C. Valmalette, M. Ezahri and A. Benlhachemi, *J. Colloid Interface Sci.*, 2020, 269–280, S0021979720304033.
7 Y. Naciri, A. Hsini, A. Bouziani, R. Djellabi, Z. Ajmal, M. Laabd, J. A. Navío, A. Mills, C. L. Bianchi, H. Li, B. Bakiz and A. Albourine, *Crit. Rev. Environ. Sci. Technol.*, 2021, DOI: 10.1080/10643389.2021.1877977.
8 M. Auta and B. H. Hameed, *Chem. Eng. J.*, 2012, **198–199**, 219–227.
9 H. Barebita, Y. Naciri, S. Ferraa, A. Nimour and T. Guedira, *Solid State Sci.*, 2020, **108**, 106389.
10 Y. Naciri, A. Hsini, Z. Ajmal, J. A. Navío, B. Bakiz, A. Albourine, M. Ezahri and A. Benlhachemi, *Adv. Colloid Interface Sci.*, 2020, **280**, 102160.
11 S. Sun, H. Yao, W. Fu, S. Xue and W. Zhang, *J. Hazard. Mater.*, 2020, **386**, 121955.
12 Y. Naciri, A. Chennah, C. Jaramillo-Páez, J. A. Navío, B. Bakiz, A. Taoufyq, M. Ezahri, S. Villain, F. Guinneton and A. Benlhachemi, *J. Environ. Chem. Eng.*, 2019, **7**, 103075.
13 Y. Naciri, H. Ait Ahsaine, A. Chennah, A. Amedlous, A. Taoufyq, B. Bakiz, M. Ezahri, S. Villain and A. Benlhachemi, *J. Environ. Chem. Eng.*, 2018, **6**, 1840–1847.
14 A. Imgharn, H. Ighnih, A. Hsini, Y. Naciri, M. Laabd, H. Kabli, M. Elamine, R. Lakhmiri, B. Souhail and A. Albourine, *Chem. Phys. Lett.*, 2021, **778**, 138811.
15 J. Vidya, A. John Bosco, K. Haribaaskar and P. Balamurugan, *Mater. Sci. Semicond. Process.*, 2019, **103**, 104645.
16 B. Ba Mohammed, A. Hsini, Y. Abdellaoui, H. Abou Oualid, M. Laabd, M. El Ouardi, A. Ait Addi, K. Yamni and N. Tijani, *J. Environ. Chem. Eng.*, 2020, **8**, 104419.
17 A. Essekri, A. Hsini, Y. Naciri, M. Laabd, Z. Ajmal, M. El Ouardi, A. Ait Addi and A. Albourine, *Int. J. Phytorem.*, 2020, 1–11.
18 A. Essekri, N. Aarab, A. Hsini, Z. Ajmal, M. Laabd, M. El Ouardi, A. Ait Addi, R. Lakhmiri and A. Albourine, *J. Dispersion Sci. Technol.*, 2020, 1–14.
19 M. Laabd, H. Chafai, N. Aarab, A. El Jaouhari, M. Bazzaoui, H. Kabli, H. Eljazouli and A. Albourine, *Environ. Chem. Lett.*, 2016, **14**, 395–400.
20 M. Laabd, A. El Jaouhari, M. Bazzaoui, A. Albourine and H. El Jazouli, *J. Polym. Environ.*, 2017, **25**, 359–369.
21 K. Pandiselvi, A. Manikumar and S. Thambidurai, *J. Appl. Polym. Sci.*, 2014, **131**, DOI: 10.1002/app.40210.
22 X. Wei, Q. Liu, H. Zhang, J. Liu, R. Chen, R. Li, Z. Li, P. Liu and J. Wang, *J. Colloid Interface Sci.*, 2018, **511**, 1–11.
23 N. Wang, J. Li, W. Lv, J. Feng and W. Yan, *RSC Adv.*, 2015, **5**, 21132–21141.
24 A. Hsini, Y. Naciri, M. Laabd, A. Bouziani, J. A. Navío, F. Puga, R. Boukherroub, R. Lakhmiri and A. Albourine, *J. Environ. Chem. Eng.*, 2021, **9**, 105885.
25 L. H. Li, J. Xiao, P. Liu and G. W. Yang, *Sci. Rep.*, 2015, **5**, 9028.
26 M. Nagpal and R. Kakkar, *Sep. Purif. Technol.*, 2019, **211**, 522–539.
27 D. Chen and J. Ye, *Adv. Funct. Mater.*, 2008, **18**, 1922–1928.
28 H. Zhang, J. Yang, D. Li, W. Guo, Q. Qin, L. Zhu and W. Zheng, *Appl. Surf. Sci.*, 2014, **305**, 274–280.
29 S. Agarwal, I. Tyagi, V. K. Gupta, F. Golbaz, A. N. Golikand and O. Moradi, *J. Mol. Liq.*, 2016, **218**, 494–498.
30 A. Muhammad, A.-H. A. Shah, S. Bilal and G. Rahman, *Materials*, 2019, **12**, 1764.
31 A. Hsini, Y. Naciri, M. Benafqir, Z. Ajmal, N. Aarab, M. Laabd, J. A. Navío, F. Puga, R. Boukherroub, B. Bakiz and A. Albourine, *J. Colloid Interface Sci.*, 2021, **585**, 560–573.
32 S. M. Ali, K. M. Emran and A. L. L. Al-Oufi, *J. Mol. Liq.*, 2017, **233**, 89–99.
33 W. Li, J. Li, X. Wang and Q. Chen, *Appl. Surf. Sci.*, 2012, **263**, 157–162.
34 A. Hsini, A. Essekri, N. Aarab, M. Laabd, A. Ait Addi, R. Lakhmiri and A. Albourine, *Environ. Sci. Pollut. Res.*, 2020, **27**, 15245–15258.
35 Y. Bu and Z. Chen, *ACS Appl. Mater. Interfaces*, 2014, **6**, 17589–17598.
36 P. Kharazi, R. Rahimi and M. Rabbani, *Solid State Sci.*, 2019, **93**, 95–100.
37 L. Liu, L. Ding, Y. Liu, W. An, S. Lin, Y. Liang and W. Cui, *Appl. Catal., B*, 2017, **201**, 92–104.
38 S. Adhikari, S. Mandal, D. Sarkar, D.-H. Kim and G. Madras, *Appl. Surf. Sci.*, 2017, **420**, 472–482.
39 M. Laabd, A. Hallaoui, N. Aarb, A. Essekri, H. Eljazouli, R. Lakhmiri and A. Albourine, *Fibers Polym.*, 2019, **20**, 896–905.
40 S. Bai, Y. Ma, R. Luo, A. Chen and D. Li, *RSC Adv.*, 2016, **6**, 2687–2694.
41 J. Jia, C. Jiang, X. Zhang, P. Li, J. Xiong, Z. Zhang, T. Wu and Y. Wang, *Appl. Surf. Sci.*, 2019, **495**, 143524.
42 M. Tanzifi, M. T. Yaraki, A. D. Kiadehi, S. H. Hosseini, M. Olazar, A. K. Bharti, S. Agarwal, V. K. Gupta and A. Kazemi, *J. Colloid Interface Sci.*, 2018, **510**, 246–261.
43 N. Wang, J. Feng, J. Chen, J. Wang and W. Yan, *Chem. Eng. J.*, 2017, **316**, 33–40.
44 P. Li, T. Fu, X. Gao, W. Zhu, C. Han, N. Liu, S. He, Y. Luo and W. Ma, *J. Chem. Eng. Data*, 2019, **64**, 2686–2696.
45 M. Laabd, H. Ait Ahsaine, A. El Jaouhari, B. Bakiz, M. Bazzaoui, M. Ezahri, A. Albourine and A. Benlhachemi, *J. Environ. Chem. Eng.*, 2016, **4**, 3096–3105.
46 B. Tanhaei, A. Ayati, M. Lahtinen and M. Sillanpää, *Chem. Eng. J.*, 2015, **259**, 1–10.
47 J. Saini, V. K. Garg, R. K. Gupta and N. Kataria, *J. Environ. Chem. Eng.*, 2017, **5**, 884–892.
48 Z. A. Sutirman, M. M. Sanagi, K. J. Abd Karim, A. Abu Naim and W. A. Wan Ibrahim, *Int. J. Biol. Macromol.*, 2019, **133**, 1260–1267.
49 H. Laksaci, A. Khelifi, B. Belhamdi and M. Trari, *Microchem. J.*, 2019, **145**, 908–913.
50 A. M. Donia, A. A. Atia, W. A. Al-amrani and A. M. El-Nahas, *J. Hazard. Mater.*, 2009, **161**, 1544–1550.
51 X. Zheng, H. Zheng, Y. Zhou, Y. Sun, R. Zhao, Y. Liu and S. Zhang, *Colloids Surf., A*, 2019, **580**, 123746.

52 O. Mahi, K. Khaldi, M. S. Belardja, A. Belmokhtar and A. Benyoucef, *J. Inorg. Organomet. Polym.*, 2021, **31**, 2095–2104.

53 A. Hsini, M. Benafqir, Y. Naciri, M. Laabd, A. Bouziani, M. Ez-zahery, R. Lakhmiri, N. E. Alem and A. Albourine, *Colloids Surf., A*, 2021, **617**, 126274.